CBN 11-3

Compact PPM Undulator for Cornell High Energy Synchrotron Source

Alexander Temnykh*, Thomas Kobela, Aaron Lyndaker, James Savino, Ethan Suttner and Yulin Li
CLASSE, Cornell University, Ithaca, NY 14850, August 9 2011

Abstract

Motivated by the needs of Cornell High Energy Synchrotron Source (CHESS), we developed and are now constructing a novel type of planar undulator magnet called CHESS Compact Undulator. The device consists of two pure permanent magnet (PPM) arrays mounted inside of a rectangular box-like frame on linear bearings providing magnet array motion along the beam axis. The outside frame dimensions are 156 mm x 148 mm. Undulator is 1 meter long. It has 5mm constant gap. The magnetic field strength is controlled by the array longitudinal motion (adjustable phase scheme). Magnetic structure has 24.4 mm period and maximum peak field 1.1 Tesla. The used PM material is Nd-Fe-B of 40UH grade.

The undulator magnet will be enclosed in a 273 mm (10.75") diameter cylindrical vacuum vessel while the driver mechanism responsible for moving the magnet array, will be placed outside.

The following sections describe mechanical and magnetic design of undulator and present results of the magnetic field measurement and evaluation of vacuum properties.

I. INTRODUCTION

UNULATOR magnets are widely used for generation of x-rays at synchrotron radiation sources. The typical undulator consists of a massive C-shape frame, two or four magnet arrays and driving mechanisms. Magnet arrays attach to the frame and driver mechanisms provide precise arrays motion. Because magnet forces between arrays are quite significant (few tons) and varying, but the tolerances on array position is quite small (few microns), the C-frame holding magnet arrays in place must be very stiff. This requirement results in large and heavy structures. The typical undulators are 2.5 m high (or higher), 1.5m wide and weighs more than ton per meter length. Note that both, dimensions and weight are driven by the frame.

We developed and built CHESS Compact undulator magnet that, while having magnetic field similar to a typical PPM planar undulators, is approximately 10 times smaller in the transverse direction and weighs around 80 kg per a meter of length. This design employs a box-shaped frame that is much stiffer than a C-shaped with internally mounted magnet arrays. To implement field control the design uses an

adjustable phase (AP) scheme developed in ref. [1]. The magnet has similarities with the device described in ref. [2].

In the following sections we describe the design of the undulator magnet, its mechanical, magnetic and vacuum properties, and report results of magnetic field measurements as well as expected properties of x-ray beam.

II. General Design

The CHESS-Compact Undulator magnet, see Fig.1, is 24.4mm period, one meter long, planar PPM undulator with maximum field ~1.1 T constructed for use in Cornell Electron Storage Ring (CESR). The magnet has rectangular box-shape frame formed by 24 mm and 34 mm thickness aluminum plates (1). Two magnet arrays are composed of base plates (4) and permanent magnet (PM) blocks (2) fastened to copper holders (3). PM arrays are mounted inside frame with 12 miniature linear bearings (5).

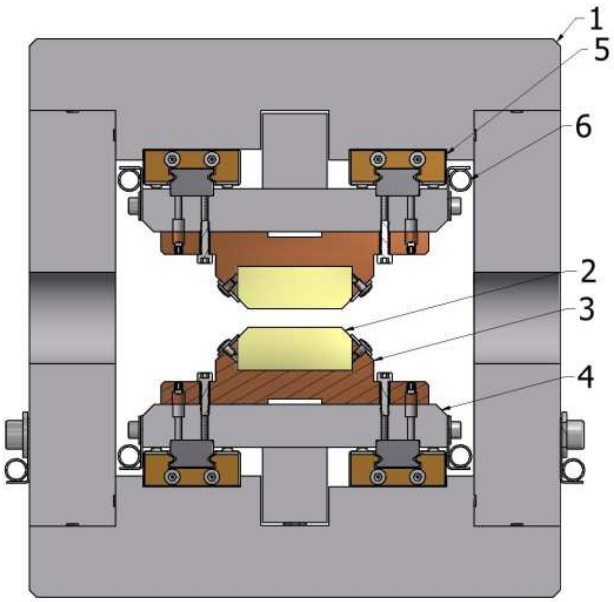

Fig. 1. CHESS Compact Undulator cross-section. (1) – thick aluminum plates comprising the undulator frame; (2) – permanent magnet blocks soldered to copper holders (3); (4) – base plates holding PM block/holder assemblies; (5) – miniature rails; (6) – cooling lines. Outer frame dimensions are 152mm x 146mm. Gap between magnets is 5mm.

The permanent magnet material used is Nd-Fe-B of 40UH grade with Br = 1.25 Tesla and Hcj = 25.0 kOe. Blocks are attached to copper holders by a soldering technique developed in ref. [3]. The holders are then constrained by 1/8" OD dowel pins and are fastened to the base plates with two #4-40 stainless steel screws.

While the lower magnet array is fixed to the frame, the upper array can be moved along beam axis by a half period (12.2mm) by a driving mechanism described in the following sections. The array motion is used to control magnetic field strength as described in ref [1]. Cooling lines attached to the magnet arrays and frame will be used to control magnet array and frame temperatures.

To minimize high-order mode power loss special cares were taken to provide smooth path for the beam image current through the magnet. PM arrays will be covered with Ni plated copper foil. Special

end assemblies provide smooth tapered transition from large, 25mm, vertical aperture to 5mm gap in undulator. The foil tension mechanism is discussed below.

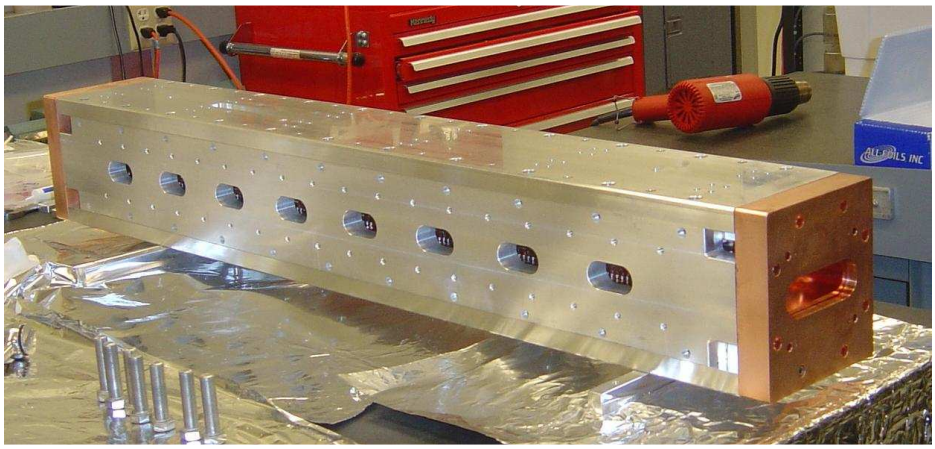

Fig. 2. CHESS Compact undulator on assembly bench.

Fig. 2 depicts the assembled undulator body on the bench. It is ~ 1.1m long, 148mm wide, 152mm high. The body will be enclosed into 273 mm (10.75") OD cylindrical vacuum vessel that is under fabrication.

III. MECHANICAL PROPERTIES

A. Frame

The frame consists of four one meter long aluminum (6061-T6 alloy) plates with 24 mm and 30 mm thickness. The total weight of the frame is around 35kg. The unique feature of the closed box-frame design is that the force loops are contained within a small, stiff structure. Where the large vertical forces typically result in a roll of the magnet girders in conventional scheme, the closed frame and lateral symmetry effectively eliminate that deformation. Finite element analysis with ANSYS Workbench, see Fig. 3, indicates a maximum frame deformation around of 1 micron under the 6.3kN of load from magnetic forces at the location of the driver slot on the top of the frame. This level of deformation is completely acceptable.

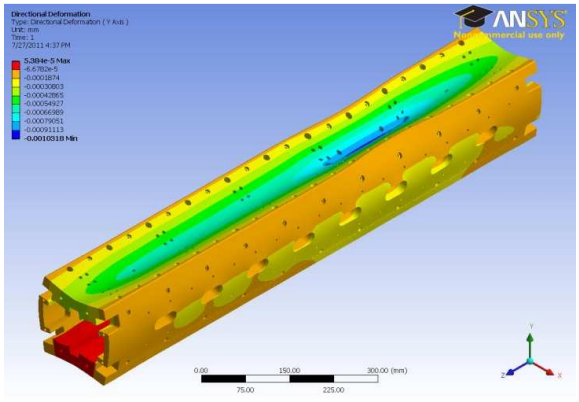

Fig. 3. Frame deformation under 6.3kN load from magnetic forces calculated with program ANSYS.

The gap change associated with the changing vertical magnetic force is primarily dominated by the stiffness of the linear bearings.

B. Driver mechanism and magnet array deformation.

The driver mechanism was designed to provide 6.3kN load (plus 30% margin) to move magnet array. Mechanism schematic with explanations is shown in Fig. 4.

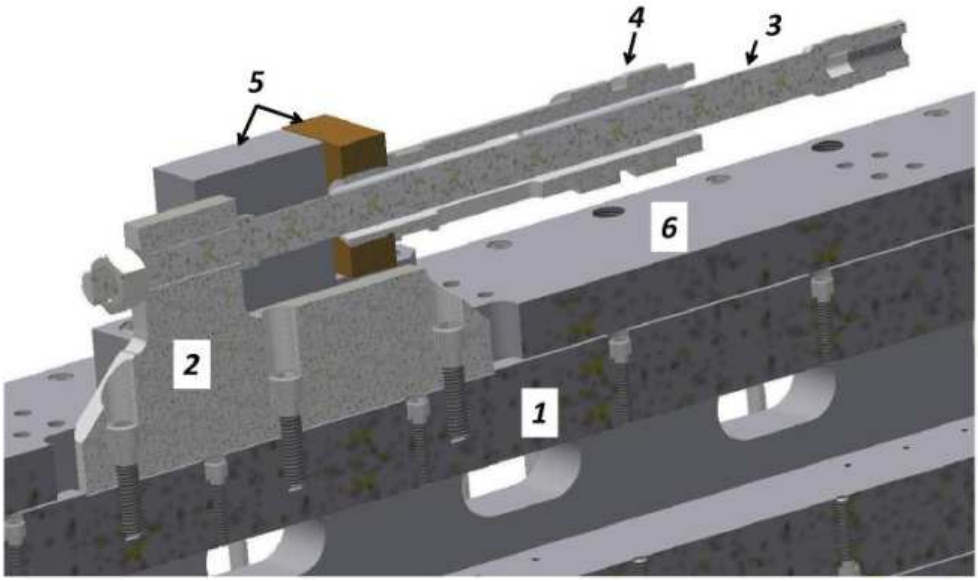

Fig. 4. Magnet array driving mechanism. The magnet array (1) is moved by a pulling a stainless steel (SS) rod (3) connected to the magnet array via a SS plate (2). The SS tube (4) attached to undulator frame (6) by the blocks (5) provides the path for the reaction forces.

It should be noted that the driving mechanism shown in Fig.4 did not include vacuum vessel. Edge-welded stainless steel bellows will be used to link the driving mechanism to a stepper motor resided outside of the vacuum vessel. Both the drive rod (3) and a concentric tube (4) pass through bellows to keep the net force on chamber and subsequently the internal undulator mounts near zero.

Due to the offset between the face of the magnets and the location of the applied force, the linear bearings must provide the reaction moment resulting in a slightly S-shape to the magnet array. To evaluate the design, finite-element analysis (using ANSYS) of the deformations and stresses on the driving linkage were calculated. Fig. 5 shows the simplified model with the predicted deformations that are primarily dominated by the stiffness of the linear bearings.

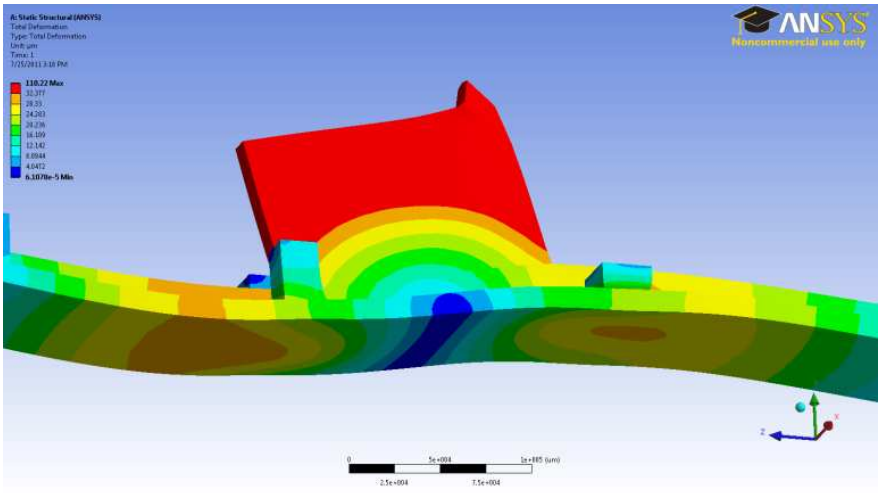

Fig. 5. The bending moment due to the driver causes an S-shape in the magnet array with a peak deformation of +/-25µm.

The peak deformation of the magnet array is +/-25µm and it occurs when the phase between two magnet arrays is at 90 degrees. Effects of this deformation on the overall undulator performance were studied and found to be acceptable for the planned application. In principal, if this deformation appears to be a problem, it can be reduced by using stiffer bearings.

C. Component Specification

The linear bearings chosen for the device are from NSK, model LU120070TRK1-PCZ1. They are a single row, profiled rail, four point contact, recirculating-ball style bearing composed primarily of 440C stainless steel. It has a static load capacity of 3.5kN and a stiffness of 33N/µm. The PTFE end caps of these bearings were replaced with custom fabricated bronze parts due to the deleterious effects of radiation on the PTFE components. All rolling elements were lubricated with ultra-high vacuum (UHV) compatible lubricant (Krytox 16256).

There are two relevant loading conditions used to size the linear bearings. The first is the maximum vertical force of 6.3kN that occurs with a zero phase between magnet arrays. By geometry, this can be assumed to be equally shared among the bearings. The more limiting case is due to the combined moment loading of the linear actuator and the equivalent vertical force. With a moment arm of 128mm, the 6.3kN driving force results in a reaction moment of 806Nm that, when shared among the four nearest bearings with a spacing of 184mm, requires a load capacity 2.2kN per bearing.

The linear actuator chosen to provide the 6.2kN of driving force and control the phase of the movable magnet array is from Danaher Motion, model EC3-T32V-70-5B-50-MF1-FT1E with 7.2kN thrust load capacity. It is comprised of a 5mm lead, non-preloaded ball-screw supported by dual preloaded angular contact bearings. Actuation is achieved with open loop stepper motor positioning through a 7:1 helical gear set. The traveling rod is guided by plain bronze linear bearings. It has a specified repeatability of 25µm and 250µm of backlash. Because the loading due to the longitudinal component of the magnetic field is unidirectional, with standard backlash correction routines in the motor controller, the lash is not problematic.

The measured input and response of the device met expectations.

D. Driver Test Results

To confirm the loads predicted by the model and to verify the mechanical behavior of the components we performed the following test of the assembled undulator, see Fig. 6.

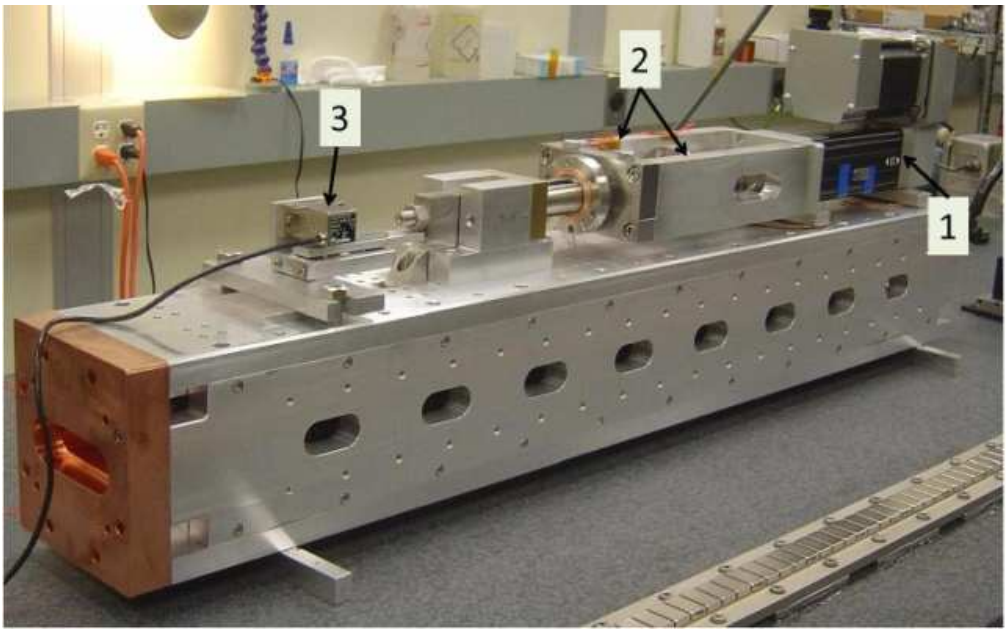

Fig. 6. Assembled undulator magnet with linear actuator (1) attached. Plates (2) connect linear actuator front plate with driver tube (4), see Fig. 4.

Two strain gages were applied to the mechanical drive critical components. One gauge was attached to the drive rod, (3) on Fig. 4, and the other to the one of the side plates, component (2) in Fig. 6. The drive rod acts in tension and each side plate acts in compression between the linear actuator and the upper array.

In the test the linear actuator moved the upper magnet array from -4mm (-59^0) to ~12.2mm (180^0) with 0.1mm (1.47^0) step. After each step we recorded gage signals. The measured dependence of the signals on the linear actuator position converted to the phase between the magnet arrays is depicted in Fig. 7.

As expected, the gages indicated opposite signs, sine like dependences with zero strains at 0^0 and 180^0. In the operating region, between 0^0 and 180^0, sensor attached to the drive rod shown tension and sensor on a side plate - compression.

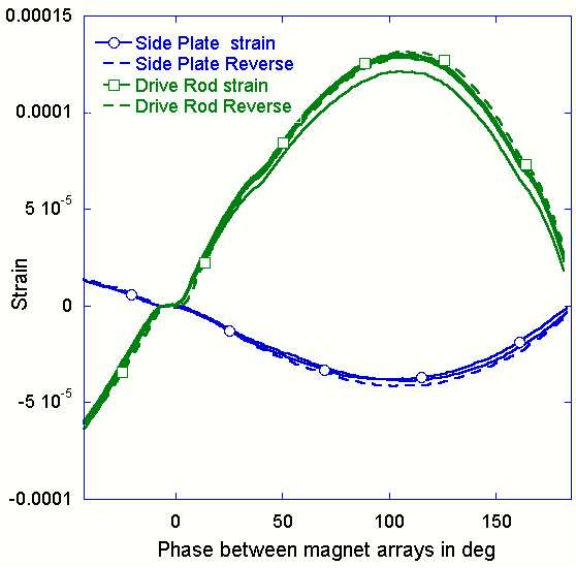

Fig. 7. The drive rod and side plates have maximum strain at 100 degrees phase with values $12.9 \cdot 10^{-5}$ and $-3.69 \cdot 10^{-5}$, respectively. This is corresponds to 31.5MPa and -2.9MPa.

Both indicated maximum tension/compression at around 100^0 phase. This phase is different from the predicted 90^0. The cause of the discrepancy is not clear and now is under investigation. The negligible difference between strains measured for forward (solid lines) and backwards (dashed lines) array motion indicates that there is no the friction contribution.

Fig. 8. Drive rod stress analysis. ANSYS predicts the measured 1.29e-5 strain at the gauge location under 5.8 kN applied force.

The data indicates the maximum strain measured on a driver rod is 12.9e-5. ANSYS predicts, see Fig.8, that this strain is the result of 31.5MPa stress or 5.8 kN load. The later is just ~9% different from the load (6.2kN) predicted in 3D magnetic modeling. The difference can be easily explained by uncertain in a strain gage calibration.

For the side plates, components (2) in Fig. 6, the ANSYS prediction for strain/stress at the gage location was -6.87e-5/-4.87MPa under 6.2kN of magnetic force load. The measured strain is only -3.7e-5, i.e., 1.7 times lower. This discrepancy can be explained by the redistribution of load between two side plates and inside of the plates due to misalignment of the components of a driver mechanism.

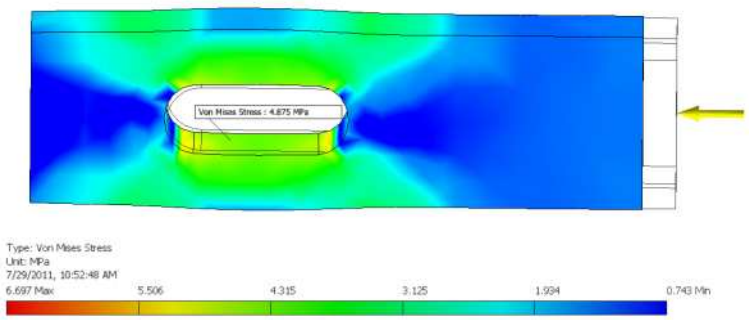

Fig. 9. Side plate stress analysis. The maximum stress in the side plate at the location of the gauge predicted by ANSYS is -4.875 MPa. The applied load is 3.1kN. For more details see text.

The good agreement between ANSYS predicted strain on the driver rod (where geometry is simple) and the measured validates the whole process of the design starting from 3D magnetic field modeling.

E. Image Current Path

A number of components maintain an electrically continuous path along the beam axis with small height variations to lessen HOM loads. Figure 10 shows an isometric view of the path at the upstream and downstream ends of the device. At the entry and exit, a copper plate maintains contact with the upstream mask through a flexible finger joint and the plate is connected to a machined copper taper through a similar finger based sliding joint. A flexible copper knife edge maintains electrical connection to a nickel plated copper foil stretched over the magnet array. When the foil grows due to thermal effects, a flexible bronze support accommodates the increased length. The tensioner mechanism can take up to 1mm in length change, equivalent to an average temperature rise of approximately 50^0C.

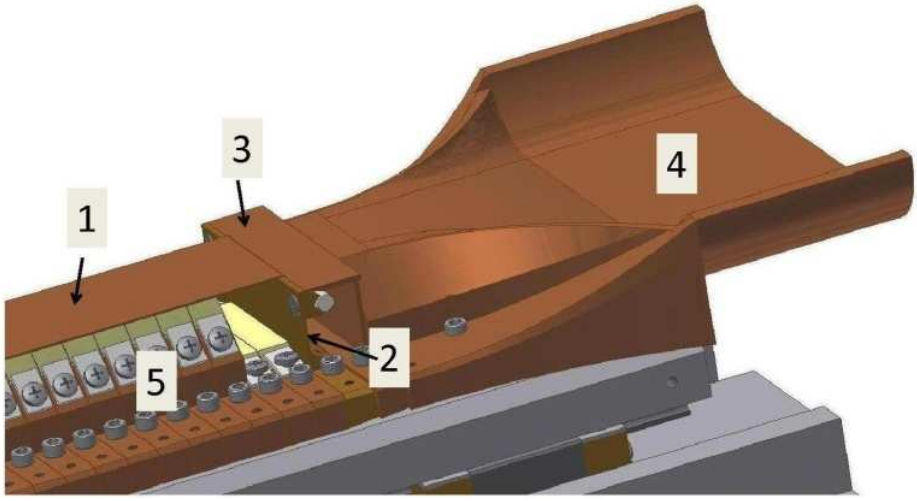

Fig. 10. A number of components maintain continuity through the device. The beam enters from the right. The end transition (4) made of a solid piece of copper provide a smooth transition from 50 mm vertical aperture outside of the undulator to the 5mm undulator gap. The transition is connected with knife shaped bridge (3) to the copper tape

(1) stretched through the magnet. Spring elements (2) provide the tape tension and accommodate the difference in thermal expansion between aluminum base plate and the tape.

F. Cooling Scheme

The magnet array is required to sink a design heat load of up to 50W due to both resistive and HOM heating. The bulk of this will occur at the tapered transitions and in the copper foil and thus must be sunk to a cooled surface without passing through the linear bearings. Two monolithic, flexible water cooling lines fabricated from bent 0.25" 316SS tubing bolt to both the magnet arrays and to the aluminum box frame. If water is used as a coolant, estimated cooling capacity of the system will be around 800W/^{0}K.

With the large diameter cooling line in relation to the total heat load, this design has the possibility to employ gas cooling with cold nitrogen gas. The gas cooled model will be able to decrease the temperature of the magnet arrays to approximately 0^{0}C or lower and thereby decrease potential demagnetization of permanent magnet blocks by radiation caused by a high energy electrons scattered from electron beam.

II. Magnetic Field Properties

A. Magnetic Field Modeling

3D magnetic field modeling was done with the program Opera from Cobham Technical Services Vector Fields Software.

For the given geometry and type of PM material used in construction the model predicted vertical peak fields 1.114T/0.818T/0 for 0^0/90^0/180^0 phases between magnet arrays respectively, see Fig. 11 left. Maximum undulator parameter K for 0^0 phase is 2.528. Calculation also predicted for these phases the alternating longitudinal magnetic field with amplitudes zero, 0.800 and 1.095T, Fig. 7 right. Note that the appearance of a longitudinal field is a feature of adjustable phase scheme.

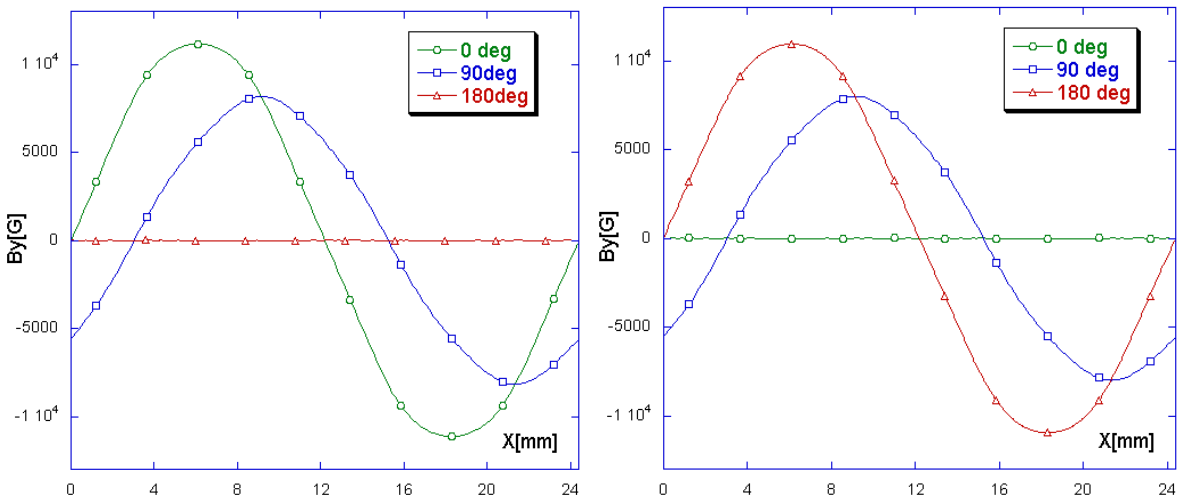

Fig. 11. Vertical (left plot) and longitudinal (right plot) magnetic field components for one undulator period calculated for 0, 90^0 and 180^0 phase between magnet arrays.

Modeling also predicted 6.3kN of vertical attractive force between magnet arrays and 6.3kN repulsive

at 0^0 and 180^0 phases shift respectively. At 90^0 phase the vertical net force is zero. Longitudinal force will have a 6.3kN maximum at 90^0 shift. At 0^0 and 180^0 phases the force is zero. It should be noted that the 0^0 phase is an equilibrium position for the magnet arrays, i.e. they will move to this position if no external forces are applied.

The normalized peak field variation as a function of horizontal δx and vertical δy offset predicted by modeling can be described as:

$$dB_y / B_y = -1.98 \times 10^{-4} \delta x^2 - 3.41 \times 10^{-6} \delta x^4$$
$$dB_y / B_y = 2.25 \times 10^{-2} \delta y^2 \qquad (1)$$

Here δx and δy are in mm. The above expressions can be used for estimation of required electron orbit stability. To provide third undulator harmonic stability $\delta\varepsilon_3 / FWHA(\varepsilon_3)$ at the 0.1 level, variation of undulator parameter K estimated with program SPECTRA should be less than 0.001. Expressions (1) imply that to provide K stability at this level, electron beam orbit at undulator should be kept in place with 0.21 mm precision in vertical plane and 2.0 mm in horizontal. This is completely feasible.

B. Magnetic Field Measurement

All magnetic field measurements were done on the field measurement bench. The bench consisted of a flat granite table and a moving carriage mounted on air-bearings and driven by linear servo motor. The motion precision was provided by the Ranishaw laser encoder. For the field profile measurement we used Hall sensor mounted on the carriage. Field integrals were measured with a long flipping coil.

Prior to assembly both magnet arrays were individually tuned to minimize optical phase errors and beam trajectory distortion. For the field analysis we used software based on MatLab scripts developed in SLAC by Zachary Wolf. The tuning was done by a small, ~0.1mm, displacement of individual magnet blocks in vertical direction.

The field quality of the assembled undulator magnet and the magnet operation were confirmed in two experiments.

In the first we used access to the magnetic field region though the vent hole in a side plate and measured the field profile in a 33 mm span for various phases/positions of the upper array. The array was moved by a stepper motor driver. Results are depicted in Fig. 12. The left plot shows the set of field profiles measured as the upper array was moved by a 1mm or 14.88^0 step starting from zero. The first, 0^0, profile indicated a maximum 1.1T peak field. The last profile taken at 169.7^0 exhibits a 0.12 T amplitude which is close to expected 0.099 T. The small difference can be explained by Hall sensor misalignment.

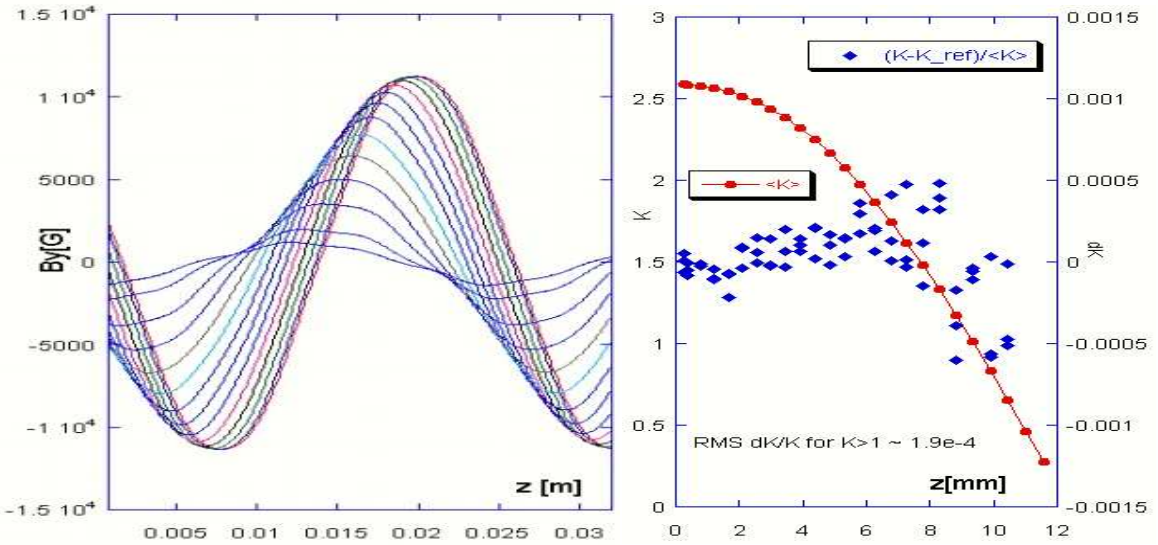

Fig. 12. Measured field profiles (left) and undulator K parameter (right) as a function of the upper array position. Plot on the right represents 4 data sets. Diamond marks indicate the measured K variation relative reference. Scale for K variation is on right side.

The measured field profiles were used to calculate undulator K parameter. The profile was approximated by a sine function with three free parameters: amplitude B_0, period λ and phase. B_0 and λ p were used to calculated K as:

$$K = 93.4 \times B_0[T] \times \lambda[m]$$

The solid circles on the right plot (left scale) depict the K parameter as a function of the array position. In this experiment, the array was moved by ~0.5mm/7.44^0 step. After each step, the field profile was measured and K parameter was calculated. The plot indicates maximum K value of 2.588 at zero phase and close to zero at 180^0. Note that the measured K maximum is approximately 2% higher than that predicted by the model, see previous section. There are two possible sources of the discrepancy; the calibration of the Hall probe and the difference between the magnetic material magnetization used in model (Br=1.26T) and the real.

To verify repeatability of the K parameter, the measurements were repeated a few times. Diamonds on the plot show the normalized K variation, dK/K, over 4 data sets relative to the first one. We used stepper motor steps as the array position variable. The data indicate the dK/K repeatability at the level of 5e-4, which is very satisfactory for the planned undulator application. The use of a precise encoder in array position control can make this repeatability better.

In the second experiment, to get full length access to the magnetic field region we temporarily removed one of the side plates and attached C-clamps, as shown in Fig. 13, to prevent frame distortion. The linear actuator was also removed and replaced by manual driver (1/2”-13 SS screw).

Fig. 13. CHESS Compact undulator on magnetic field measurement bench. To provide access to field region over all undulator length, one side plate was temporally removed and C-clamps were installed.

In this arrangement, we measured the vertical magnetic field along the beam axis for various upper array positions as well as the vertical field variation in the horizontal and vertical directions.

Fig. 10 depicts vertical magnetic field versus position along the magnet for 0^0, 93.7^0 and 177.6^0 phases. In the first case, the averaged peak field was 1.1177T, which is in very good agreement with the model prediction. At 93.7^0, the measurement indicated a 0.7603T averaged peak field which is also consistent with the model. The RMS optical phase errors for both, the 0^0 and 93.7^0 fields, were around 3.4^0.

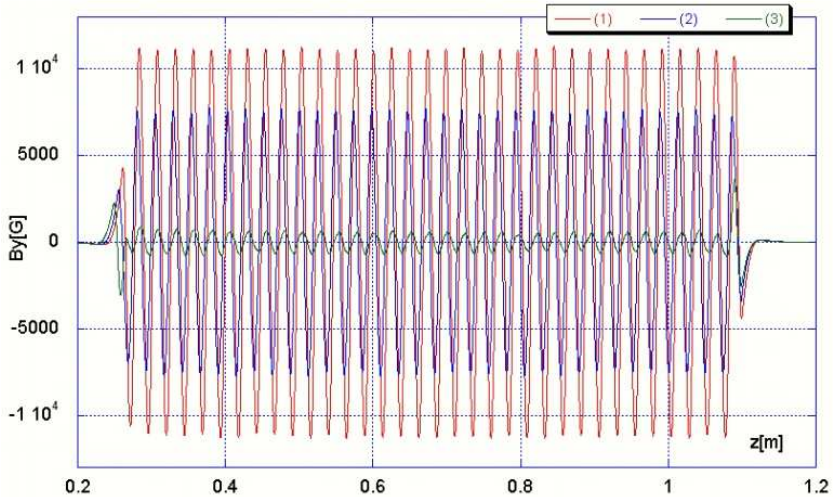

Fig. 14. Vertical magnetic field along beam axis measured for various phase between magnet arrays. (1) – phase =0, <Bpeak>=1.1177T, K=2.53633; (2) – phase=93.7^0; <Bpeak> = 0.7603 T, K= 1.732; (3) – phase=177.6^0, <Bpeak>~0.05T, K~0.011.

To demonstrate that the field quality is adequate for the planned application, we calculated the x-ray

flux density as function of photon energy using the electron beam parameters expected in CESR undulator optics for the measured and ideal fields and compared them. Results are plotted in Fig. 15. To illustrate the anticipated gain, we added the flux generated by G-line wiggler in the present conditions.

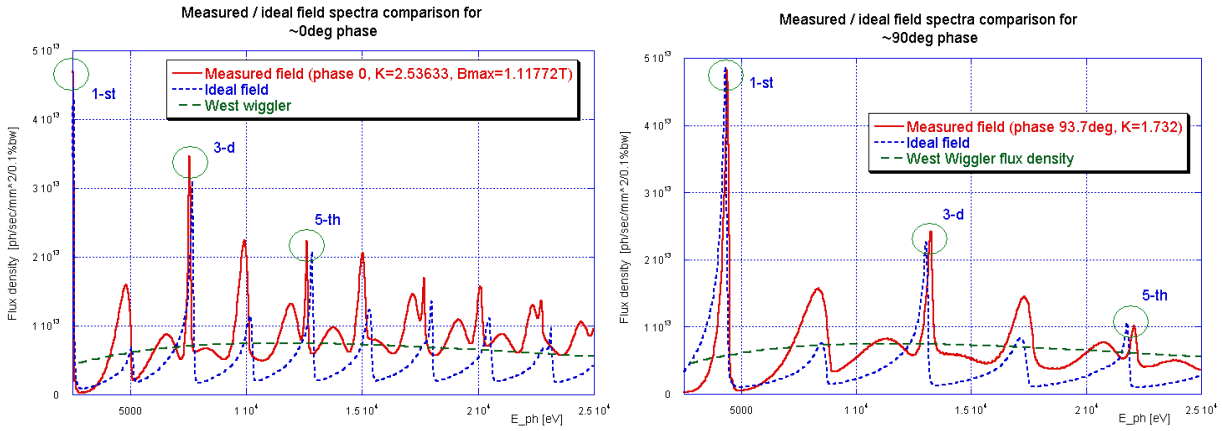

Fig. 15. X-ray flux density spectra calculated for measured field at zero phases (upper plot) and 93.7deg phase (lower plot) between magnet arrays in comparison with ideal field spectra. The calculation was made with program SPECTRA [4] using the electron beam parameters expected in CESR optics optimized for operation with undulator magnets.

Small difference between flux densities at 1-st, 3-d and 5-th undulator harmonics calculated for measured and ideal fields confirms that the undulator field is satisfactory.

We measured the field roll-off in the horizontal direction for all 68 poles and found that the variation can be described as

$$dB_y / B_y = -(1.98 \pm 0.49) \times 10^{-4} \delta x^2 - (3.42 \pm 0.63) \times 10^{-6} \delta x^4$$

where δx is in mm. Mean values of the measured coefficients agree with predicted (see previous section) insuring that the averaged dimensions of the permanent magnet blocks consist with the dimensions used in model and that the tolerance on the beam orbit stability derived from the model field is relevant. It should be noted that the relatively large spread in coefficients is due to real spread in the magnet blocks.

In the course of the field characterization, at one pole we measured vertical magnetic field as a function of vertical position for 0^0 and ~180^0 phases between arrays. Results in compare with model prediction are shown on Fig. 16.

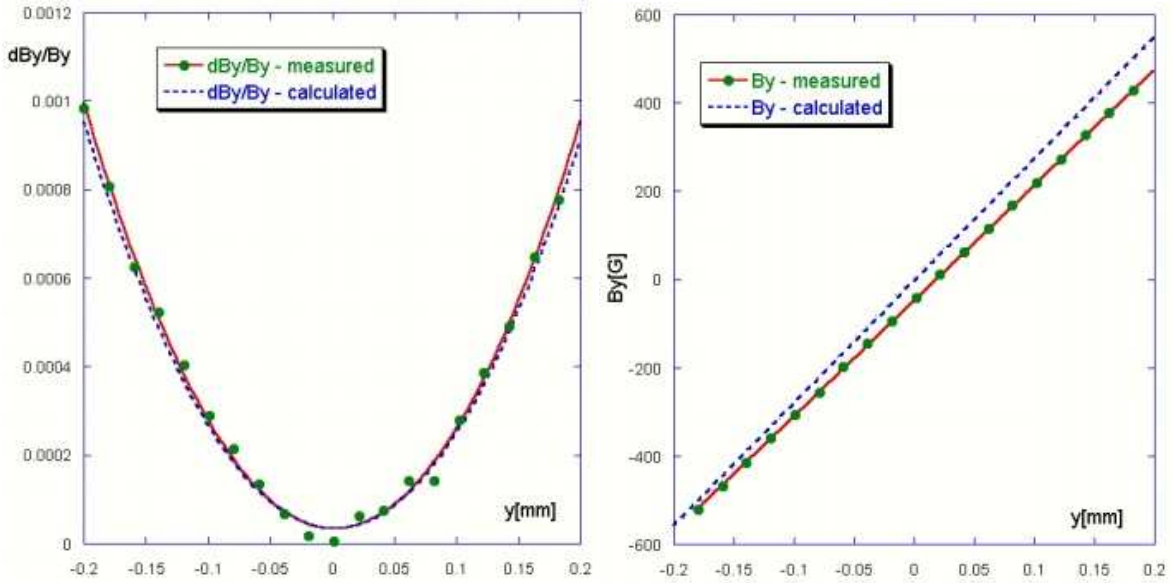

Fig. 16. Measured and predicted variations of vertical magnetic field versus vertical position at 0^0 and 180^0 phases between magnet arrays.

At 0^0 phase and small distance, Fig. 16 left, the observed normalized field variation can be fitted by a quadratic function

$$dB_y / B_y = (2.35 \pm 0.04) \times 10^{-2} \delta y^2$$

well consistent with prediction, see previous section.

At 180^0 phase the model predicted zero vertical field on the axis and the linear dependence of the field on vertical position with slope $dB_y / dy = 2768\ G / mm$. The measured slope, see Fig. 16 right, is $2617 \pm 4\ G / mm$, which is also reasonably close to the predicted value.

III. VACUUM PROPERTIES

The vacuum properties of the in-vacuum undulator are critical, as the undulator magnet will be part of the CESR UHV system. To evaluated vacuum properties of the undulator magnets both fully assembled magnet arrays were baked in special constructed vacuum vessel. Fig. 13 depicts both, temperature and pressure records taking during baking out process.

To evaluated vacuum properties of the undulator magnets both magnet arrays were baked in special constructed vacuum vessel. Fig. 17 depicts both, temperature and pressure records taking during baking out process.

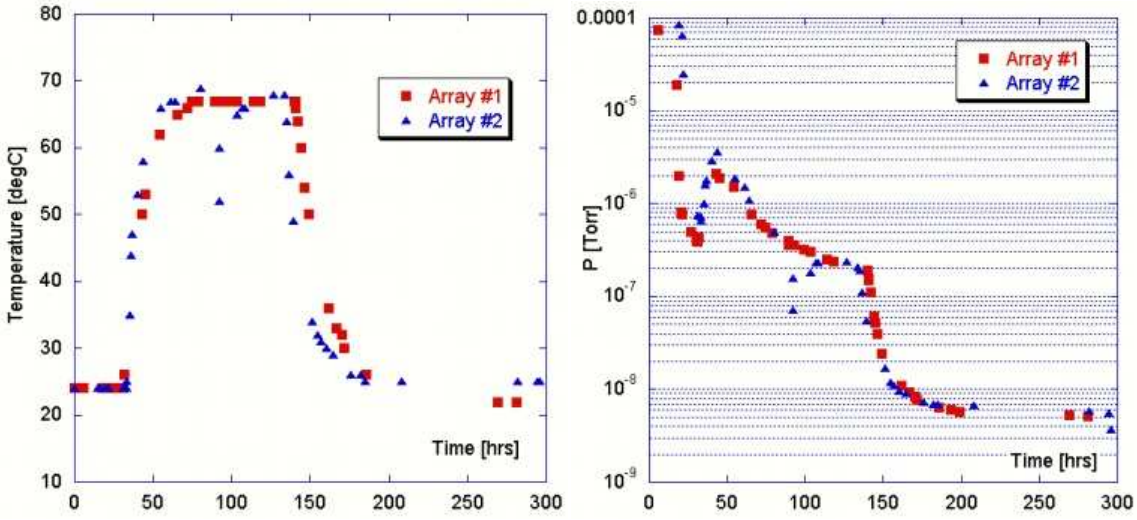

Fig. 17. Magnet array in-vacuum baking record. Left – temperature profile, right – measured pressure.

To minimize potential damage (demagnetization) of the PM blocks by elevated temperature, the baking temperature was limited to 70^0C. The baking time was ~100hrs. The vacuum pumping during the vacuum tests was provided by a turbo-molecular pump and 75l/sec ion pump. An ultimate pressure of ~5×10^{-9} torr was reached after the bakeout for both magnet arrays. Residual gas analyzer (RGA) data also showed very clean mass spectra, dominated by hydrogen, see Fig. 18.

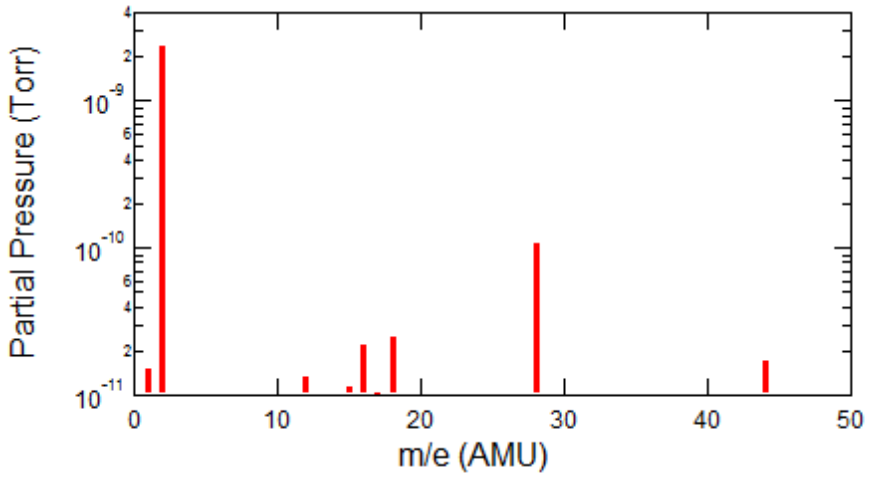

Fig. 18. RGA spectra recorded at the end of second magnet array baking cycle.

To further evaluate vacuum outgassing of the baked magnet arrays, a rate-of-rise measurement was done after the bakout. With all pumps tuned off, we observed 2.6 nTorr/sec of the rate of pressure rise. With this measured rate-of-rise and 38.4 liters of vacuum vessel volume, the outgassing rate for one magnet array is estimated to be ~1.0×10^{-7} Torr*liter/sec.

In the planned beam tests in CESR, the undulator vacuum vessel will be equipped with a 150 l/s ion pump and a large non-evaporable getter (NEG) pump. These pumps will provide a total hydrogen pumping speed of ~2000 l/s. A pair of UHV RF-shielded gate valves will be mounted at the ends of the

undulator vacuum vessel, and a pre-installation 70°C bakeout will be carried out. With the measured outgassing rate and the installed vacuum pumping, a vacuum level of $<1\times10^{-9}$ torr is expected, thus suitable for the beam tests in CESR.

IV. Conclusion

We developed, constructed and bench tested a new type of PPM planar undulator magnet (CHESS-Compact) that has significantly smaller dimensions and weight than conventional undulators operated at storage rings. The magnet is planned to be beam tested and then permanently installed at Cornell Electron Storage Ring. This type of undulator magnet can also be used at other facilities.

Acknowledgment

The authors thank Sol Gruner for his constant attention to the project and David Rice and Don Bilderback for support.

Work was supported by NSF awards DMR-0936384 and DMR-0807731.

References

[1] Carr, Nucl. Instrum. Methods Phys. Res., Sect. A 306, 391 (1991)
[2] A. Temnykh et al., Delta undulator model: Magnetic field and beam test results, Nucl. Instrum. Methods Phys. Res., Sect. A, Article in Press, Corrected Proof, doi:10.1016/j.physletb.2003.10.071
[3] A. Temnykh, US Patent 7,896,224
[4] T. Tanaka and H. Kitamura, J. Synchrotron Radiation 8 (2001) 1221